18th International Conference on Information Fusion
Washington, DC - July 6-9, 2015

IMU Alignment for Smartphone-based Automotive Navigation

Johan Wahlström, Isaac Skog, and Peter Händel
ACCESS Linnaeus Center, Dept. of Signal Processing
KTH Royal Institute of Technology
Stockholm, Sweden
Email: {jwahlst, skog, ph}@kth.se

***Abstract*—Recent years have seen an increasing interest in making use of the smartphone as a cheap and viable navigation device for land-vehicles. However, smartphone-based automotive navigation suffers from the fact that the orientation of the smartphone's inertial measurement unit, with respect to the vehicle, in general is unknown. In this study, we present a method for simultaneous vehicle navigation and smartphone-to-vehicle alignment. In addition to the state estimates obtained from applying a standard global navigation satellite system-aided inertial navigation system to estimate the smartphone dynamics, this will also provide us with estimates of the vehicle's attitude. These estimates are used to improve the navigation solution, and also enables the estimation of additional vehicle, road, and driver characteristics, which requires knowledge of the vehicle's attitude. The performance of the proposed method is evaluated with both simulations and experimental data.**

***Index Terms*—Inertial navigation systems, Smartphone sensors, GNSS-aided INSs, IMU alignment.**

I. Introduction

The navigation of land-vehicles using vehicle-fixed sensors is a mature technology with numerous commercial applications [1]. One of the current challenges of the intelligent transportation systems society lies in extending these navigation systems to implementations which can be based solely on measurements from cheap and readily accessible devices such as smartphones.

The processing power of commercial smartphones has in the past years increased at a fast pace. In addition, smartphones have been equipped with more and more features, and today typically include both a low-cost global navigation satellite system (GNSS) receiver, and an inertial measurement unit (IMU). All in all, the modern smartphone is capable of functioning as a portable and user-friendly navigation device or measurement probe for vehicles in many settings and environments. Promising applications can be found in the fields of traffic state estimaton [2], fleet management [3], advanced driver-assistance systems [4], and insurance telematics [5].

As opposed to when using vehicle-fixed sensors, smartphone-based vehicle navigation suffers from the fact that the orientation of the smartphone's IMU, with respect to the vehicle, in general is unknown. In this study, we show how to align the smartphone with respect to the vehicle, without the use of reference data. The motivation for this is twofold. First, knowing the relative orientation of the smartphone and the vehicle, it is possible to utilize constraints on the vehicle dynamics to improve the navigation solution. Second, this also enables the estimation of vehicle, road, or driver characteristics, which requires knowledge of the vehicle's attitude.

Reproducible research: The simulated and real-world data used in this paper is available at www.kth.se/profile/jwahlst/ together with a Matlab implementation of the proposed method.

II. Problem Formulation

The implementation of a GNSS-aided inertial navigation system (INS) for smartphone-based automotive navigation poses several challenges. Typically, relevant design choices involve a trade-off between ease of use, which pays off in terms of commercial viability, and navigation performance. Many of the smartphone-based GNSS-aided INSs presented in the literature put restrictions on both the smartphone usage while driving [6], and on the vehicle motion during initialization [7]. Some implementations also make use of additional data coming from more expensive and logistically demanding sources (such as the vehicle's on-board-diagnostics system or vehicle-aligned IMUs) to e.g., estimate the smartphone-to-vehicle orientation [8]. In the following, we discuss these issues in more detail.

One of the most challenging aspects of smartphone-based vehicle navigation is the question of how to separate the dynamics of the smartphone from the dynamics of the vehicle. So far, published studies have generally assumed that the smartphone is fixed with respect to the vehicle (see e.g., [6], [7], [8]). A simple way to generalize frameworks based on this assumption is to implement a detector that attempts to detect when the smartphone is non-stationary with respect to the vehicle [9]. All data obtained during the detected period is then discarded, after which the relative attitude of the smartphone must be re-estimated. The success of an implementation of this kind to a large extent depends on the navigation system's ability to perform an in-motion smartphone-to-vehicle alignment. An obvious disadvantage of this approach is that all data will be lost during the detected period, which in e.g., insurance telematics applications might encourage fraudulent behavior through excessive smartphone interaction when the driver do not wish to share driving data.

The smartphone-to-vehicle orientation is typically estimated by first assuming that the vehicle is horizontally aligned during the initialization period, so that the vehicle's roll and pitch angles relative to a tangent frame both are zero. Assuming that the vehicle does not experience any acceleration, the smartphone's roll and pitch angles can be estimated from accelerometer measurements of the gravity vector. The smartphone's yaw angle can then be identified using magnetometer measurements, while the vehicle's yaw angle is estimated using GNSS measurements of planar course [10]. Alternatively, one can directly estimate the relative yaw angle of the smartphone and the vehicle by studying accelerometer measurements during pronounced acceleration [6] or deceleration [9].

Measurements from IMUs that are rigidly attached to the vehicle, with its axes aligned to the vehicle frame, have been used for many purposes besides navigation. These include driver recognition and maneuver classification [11], detection of road bumps [12], and detection of additional roof load [13]. Relaxing the assumption of a vehicle-aligned IMU, it is possible to expand the application area of any of these frameworks.

If constraints on the true navigation state are known, these can be used to reduce the vector space of possible navigation solutions, which will improve the performance of the navigation system. In low-cost automotive navigation, the most commonly applied constraints restrict the vehicle's velocity to be approximately zero in directions perpendicular to the forward direction of the vehicle frame [14]. These are often referred to as non-holonomic constraints (NHCs), i.e., constraints on the vehicle's velocity.

In this paper, we propose a method for simultaneous vehicle navigation and smartphone-to-vehicle alignment, which can be seen as an extension of the standard GNSS-aided INS. The alignment is performed by applying NHCs with the smartphone-to-vehicle orientation as an unknown state element. The relative orientation can then be recursively estimated in a Kalman filter. The navigation system is well-suited for a real-time implementation, and requires no pre-calibration of the smartphone sensors.

The proposed method is evaluated in a simulation study which randomizes the smartphone-to-vehicle orientation and the sensor errors. In addition, we show the results of a field study where driving data from several ubiquitous devices are compared to reference data. Convergence of the estimated smartphone-to-vehicle orientation is shown to occur within minutes, and the accuracy of the estimated vehicle attitude is in the order of $2\,[^\circ]$ for each Euler angle. It is further demonstrated that the method reduce the position error growth during GNSS outages.

III. State-Space Model

In this section, the navigation problem discussed in the preceding section is formulated as a constrained nonlinear filtering problem. First, we present the navigation equations and measurements used in the standard GNSS-aided INS. The navigation state is then augmented with the relative smartphone-to-vehicle orientation, after which constraints on the vehicle motion are employed to introduce a coupling between the smartphone dynamics and the relative smartphone-to-vehicle orientation.

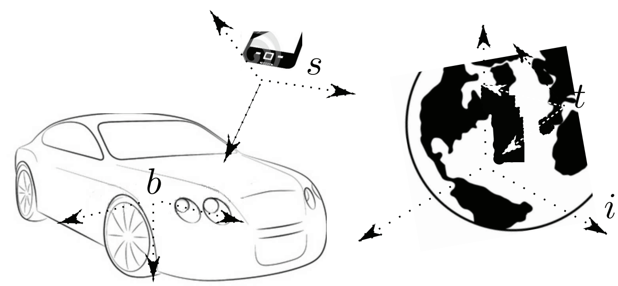

Fig. 1. The employed coordinate frames: body frame b; smartphone frame s; tangent frame t; earth-centered inertial frame i.

Values of the generic variable $\mathbf{c}$ will throughout the paper be separated as measured $\tilde{\mathbf{c}}$, estimated $\hat{\mathbf{c}}$, or developing in discrete time $\mathbf{c}_k$, where k (often omitted for notational convenience) is the index of the sampling instance T_k. Further, $\hat{\mathbf{c}}_{k_1|k_2}$ denotes the estimate of $\mathbf{c}_{k_1}$ using GNSS measurements up until T_{k_2}. We let $\mathbf{c}^{\kappa_3}_{\kappa_2\kappa_1}$ denote the physical quantity $\mathbf{c}$ of frame κ_1 with respect to frame κ_2, resolved in frame κ_3. Naturally, $\mathbf{c}^{\kappa_3}_{\kappa_2\kappa_1,k}$ refers to $\mathbf{c}^{\kappa_3}_{\kappa_2\kappa_1}$ at sampling instance T_k. The coordinate frames (see Fig. 1) are denoted by b (forward-right-down body frame, also known as the vehicle frame), s (smartphone frame), t (north-east-down tangent frame), and i (earth-centered inertial frame).

We begin by presenting the navigation equations and measurement equations commonly employed in low-cost GNSS-aided INSs. These navigation systems propagate the navigation solution using high-rate IMU measurements, and then bound the resulting navigation errors using GNSS measurements available at a lower rate. Refer to e.g., [15] and [16] for details.

Let the navigation state be defined as

$$\bar{\mathbf{z}} \triangleq [(\mathbf{r}^t_{ts})^\intercal \;\; (\mathbf{v}^t_{ts})^\intercal \;\; (\boldsymbol{\psi}^t_{ts})^\intercal]^\intercal \tag{1}$$

where $\mathbf{r}$ and $\mathbf{v}$ denote three dimensional position and velocity, respectively, and the superscript $(\cdot)^\intercal$ denotes the transpose of a matrix. Further, the roll, pitch, and yaw angle are elements in $\boldsymbol{\psi}^t_{ts} \triangleq [\phi^t_{ts} \quad \theta^t_{ts} \quad \psi^t_{ts}]^\intercal$. The input vector $\mathbf{u}$ is given by

$$\mathbf{u} \triangleq [(\mathbf{a}^s_{is})^\intercal \;\; (\boldsymbol{\omega}^s_{is})^\intercal]^\intercal \tag{2}$$

where $\mathbf{a}^s_{is}$ and $\boldsymbol{\omega}^s_{is}$ denote specific force and angular velocity, respectively. The state-space model describing the time development of the navigation state, and the GNSS measurements, is typically formulated as

$$\bar{\mathbf{z}}_{k+1} = \mathbf{f}^{\text{NE}}_k(\bar{\mathbf{z}}_k, \mathbf{u}_k), \tag{3a}$$
$$\mathbf{y}_k = \mathbf{h}^{\text{GNSS}}(\bar{\mathbf{z}}_k) + \boldsymbol{\epsilon}_k. \tag{3b}$$

Refer to [16] for details on the mechanized navigation equations $\mathbf{f}^{\text{NE}}$. (In practice, process noise have to be considered in (3a) since the input $\mathbf{u}$ cannot be measured perfectly.) The

GNSS measurements of position, speed, and planar course, are modeled as

$$\mathbf{h}^{\text{GNSS}}(\bar{\mathbf{z}}) \triangleq \big[(\mathbf{r}_{ts}^t)^\intercal \;\; \bar{\mathrm{v}}_{ts}^t \;\; \mathrm{atan2}\big([\mathbf{v}_{ts}^t]_2, [\mathbf{v}_{ts}^t]_1\big)\big]^\intercal \tag{4}$$

where the horizontal speed is defined as

$$\bar{\mathrm{v}}_{ts}^t \triangleq \sqrt{([\mathbf{v}_{ts}^t]_1)^2 + ([\mathbf{v}_{ts}^t]_2)^2} \tag{5}$$

and $[\mathbf{c}]_i$ denotes element i in $\mathbf{c}$. The measurement noise $\boldsymbol{\epsilon}$ is assumed to be white with covariance matrix [17]

$$\begin{aligned}\mathbf{R}^{\text{GNSS}} &\triangleq \mathrm{Cov}(\boldsymbol{\epsilon}) \\ &= \mathrm{blkdiag}\big(\sigma_{\mathrm{r}}^2\,\mathbf{I}_2,\ \sigma_{\mathrm{r,vert}}^2,\ \sigma_{\bar{\mathrm{v}}}^2,\ \sigma_{\bar{\mathrm{v}}}^2/(\bar{\mathrm{v}}_{ts}^t)^2\big).\end{aligned} \tag{6}$$

Here, $\mathrm{blkdiag}(\cdot, ..., \cdot)$ denotes the blockdiagonal matrix with block matrices given by the arguments, and $\mathbf{I}_n$ is the identity matrix of dimension n. Using (3), it is possible to implement a GNSS-aided INS that recursively estimates the smartphone dynamics, see e.g., [15].

Augmenting the navigation state with the Euler angles relating the smartphone frame to the vehicle frame, we obtain the augmented navigation state

$$\mathbf{z} = [\bar{\mathbf{z}}^\intercal \;\; (\boldsymbol{\psi}_{sb}^s)^\intercal]^\intercal. \tag{7}$$

To make the corresponding augmented system observable, the GNSS measurements need to be complemented with additional measurements or constraints. One possibility is to utilize that the vehicle's velocity typically is close to zero in the lateral and up/down directions of the vehicle frame [14]. To this end, we introduce the NHCs

$$\mathbf{g}^{\mathrm{v}}(\mathbf{z}) \leq \mathbf{d}^{\mathrm{v}} \tag{8}$$

where $\mathbf{d}^{\mathrm{v}}$ is some constant, while $\mathbf{g}^{\mathrm{v}}(\mathbf{z}) \triangleq |\mathbf{A}\mathbf{v}_{tb}^b|$ and $\mathbf{A} \triangleq [\mathbf{0}_{2,1} \;\; \mathbf{I}_2]$ with $\mathbf{0}_{n_1,n_2}$ denoting the zero matrix of dimension $n_1 \times n_2$. Further, $\leq$ and $|\cdot|$ are used to denote component-wise inequality and absolute value, respectively.

Moreover, we note that the vehicle's roll angle typically varies around zero without any large deviations, leading us to introduce the additional constraint

$$\mathbf{g}^{\phi}(\mathbf{z}) \leq \mathbf{d}^{\phi} \tag{9}$$

where $\mathbf{d}^{\phi}$ is some constant, while $\mathbf{g}^{\phi}(\mathbf{z}) \triangleq |\mathbf{b}^\intercal \boldsymbol{\psi}_{tb}^t|$ and $\mathbf{b} \triangleq [1 \;\; 0 \;\; 0]^\intercal$.

The state-space model (3) and the dynamic constraints (8) and (9) can be summarized by the new system model

$$\mathbf{z}_{k+1} = \mathbf{f}_k(\mathbf{z}_k, \mathbf{u}_k) + \mathbf{w}_k, \tag{10a}$$

$$\mathbf{y}_k = \mathbf{h}(\mathbf{z}_k) + \boldsymbol{\epsilon}_k, \tag{10b}$$

and the constraints

$$\mathbf{g}(\mathbf{z}_k) \leq \mathbf{d}. \tag{10c}$$

We have here assumed that $\mathbf{h}(\mathbf{z}) \triangleq \mathbf{h}^{\text{GNSS}}(\bar{\mathbf{z}})$ and $\mathbf{f}_k(\mathbf{z}_k, \mathbf{u}_k) \triangleq [(\mathbf{f}_k^{\text{NE}}(\bar{\mathbf{z}}_k, \mathbf{u}_k))^\intercal \, (\mathbf{f}^{\psi}(\mathbf{z}_k, \mathbf{u}_k))^\intercal]^\intercal$, where $\mathbf{f}^{\psi}$ is some function describing the time development of $\boldsymbol{\psi}_{sb,k}^s$. Further, we have made use of the definitions $\mathbf{g}(\mathbf{z}) \triangleq [(\mathbf{g}^{\mathrm{v}}(\mathbf{z}))^\intercal \;\; \mathbf{g}^{\phi}(\mathbf{z})]^\intercal$ and $\mathbf{d} \triangleq [(\mathbf{d}^{\mathrm{v}})^\intercal \;\; \mathbf{d}^{\phi}]^\intercal$. The problem of estimating $\mathbf{z}$ from (10) defines a constrained nonlinear filtering problem which can be approached by several methods. One alternative is to formulate the constraints (10c) as pseudo observations and then linearize the system in an extended Kalman filter (EKF) [18]. This method is considered next.

IV. EKF-based Navigation System

In what follows, we present an EKF-based solution to the constrained nonlinear filtering problem presented in the preceding section. First, the navigation equations are linearized around the estimated motion dynamics and the IMU measurements. The state constraints are then re-formulated as pseudo observations that extend the measurement equation, after which also the measurement equation is linearized. The resulting state-space model forms the basis of an EKF which provides estimates of the vehicle dynamics. The section concludes with a discussion on filter initialization.

A. Model of the System Error Dynamics

We begin by defining the error vector

$$\mathbf{x} \triangleq \big[(\delta\mathbf{z})^\intercal \;\; (\delta\mathbf{u})^\intercal\big]^\intercal \tag{11}$$

where $\delta\mathbf{z} \triangleq \big[(\delta\mathbf{r}_{ts}^t)^\intercal \; (\delta\mathbf{v}_{ts}^t)^\intercal \; (\delta\boldsymbol{\psi}_{ts}^t)^\intercal \; (\delta\boldsymbol{\psi}_{sb}^s)^\intercal\big]^\intercal$. In addition to the estimation errors $\delta\mathbf{r}_{ts}^t \triangleq \hat{\mathbf{r}}_{ts}^t - \mathbf{r}_{ts}^t$, $\delta\mathbf{v}_{ts}^t \triangleq \hat{\mathbf{v}}_{ts}^t - \mathbf{v}_{ts}^t$, $\delta\boldsymbol{\psi}_{ts}^t$, and $\delta\boldsymbol{\psi}_{sb}^s$ (the last two of which are defined by (19) in the Appendix), the error vector also include the IMU bias $\delta\mathbf{u}$. Note that $\mathbf{x}$ can be obtained as a straightforward extension of the 15-state error vector in the standard GNSS-aided INS framework (see e.g., [16]).

Linearizing (10a) around $\hat{\mathbf{z}}$ and $\tilde{\mathbf{u}}$, the time development of $\mathbf{x}$ can be described by

$$\mathbf{x}_{k+1} = \boldsymbol{\Phi}_k \mathbf{x}_k + \mathbf{G}_k \mathbf{w}_k \tag{12}$$

where the process noise covariance is $\mathrm{Cov}(\mathbf{w}_k) = \mathbf{Q}_k$ (see e.g., [15] for example derivations and definitions of filter matrices). The implementation considered here models $\boldsymbol{\psi}_{sb,k}^s$ as a random walk.

We now reformulate the dynamics constraints (10c) as the pseudo observations

$$\mathbf{0}_{2,1} = \mathbf{h}^{\mathrm{ps,v}}(\mathbf{z}_k) + \boldsymbol{\epsilon}_k^{\mathrm{ps,v}}, \tag{13a}$$

$$0 = \mathbf{h}^{\mathrm{ps},\phi}(\mathbf{z}_k) + \boldsymbol{\epsilon}_k^{\mathrm{ps},\phi}, \tag{13b}$$

where $\mathbf{h}^{\mathrm{ps,v}}(\mathbf{z}) \triangleq \mathbf{A}\mathbf{v}_{tb}^b$ and $\mathbf{h}^{\mathrm{ps},\phi}(\mathbf{z}) \triangleq \mathbf{b}\boldsymbol{\psi}_{tb}^t$. The measurement errors $\boldsymbol{\epsilon}^{\mathrm{ps,v}}$ and $\boldsymbol{\epsilon}^{\mathrm{ps},\phi}$ are modeled as white with covariance matrices $\mathbf{R}^{\mathrm{ps,v}} \triangleq \sigma_{\mathrm{ps,v}}^2 \mathbf{I}_2$ and $\mathbf{R}^{\mathrm{ps},\phi} \triangleq \sigma_{\mathrm{ps},\phi}^2$, respectively. For notational convenience, the measurement function and the measurement noise covariance matrix for the complete set of pseudo observations are denoted by $\mathbf{h}^{\mathrm{ps}}(\mathbf{z}) \triangleq [(\mathbf{h}^{\mathrm{ps,v}}(\mathbf{z}))^\intercal \;\; \mathbf{h}^{\mathrm{ps},\phi}(\mathbf{z})]^\intercal$ and $\mathbf{R}^{\mathrm{ps}} \triangleq \mathrm{blkdiag}(\mathbf{R}^{\mathrm{ps,v}}, \mathbf{R}^{\mathrm{ps},\phi})$, respectively.

Linearizing the GNSS measurement equations (10b) and the pseudo observations (13) around $\hat{\mathbf{z}}$ and $\tilde{\mathbf{u}}$, we obtain the measurement equation (see the Appendix)

$$\delta\mathbf{y}_k = \mathbf{H}_k \mathbf{x}_k + \mathbf{e}_k \tag{14}$$

Algorithm 1 : EKF-based navigation algorithm.

1: Perform a Kalman filter time update using (3a) and (12). The navigation state errors are set to zero as the navigation solution is updated in the last step of the algorithm.

$$\begin{aligned}\hat{\mathbf{z}}_{k+1|k} &= \mathbf{f}_k(\hat{\mathbf{z}}_{k|k}, \tilde{\mathbf{u}}_k - \delta\hat{\mathbf{u}}_{k|k}),\\ \mathbf{P}_{k+1|k} &= \mathbf{\Phi}_k \mathbf{P}_{k|k} \mathbf{\Phi}_k^\intercal + \mathbf{G}_k \mathbf{Q}_k \mathbf{G}_k^\intercal,\\ \hat{\mathbf{x}}_{k+1|k} &= [\mathbf{0}_{1,12}\ (\delta\hat{\mathbf{u}}_{k|k})^\intercal]^\intercal.\end{aligned}$$

2: If there are GNSS measurements at T_{k+1}, use (14) to perform a Kalman filter measurement update utilizing GNSS measurements, and pseudo observations of velocity and roll:

$$\begin{aligned}\mathbf{S}_{k+1} &= \mathbf{H}_{k+1}\mathbf{P}_{k+1|k}\mathbf{H}_{k+1}^\intercal + \mathbf{R}_{k+1},\\ \mathbf{K}_{k+1} &= \mathbf{P}_{k+1|k}\mathbf{H}_{k+1}^\intercal \mathbf{S}_{k+1}^{-1},\\ \hat{\mathbf{x}}_{k+1|k+1} &= \hat{\mathbf{x}}_{k+1|k} + \mathbf{K}_{k+1}\delta\mathbf{y}_{k+1},\\ \mathbf{P}_{k+1|k+1} &= (\mathbf{I}_{18} - \mathbf{K}_{k+1}\mathbf{H}_{k+1})\mathbf{P}_{k+1|k}.\end{aligned}$$

3: If there are no GNSS measurements at T_{k+1}, use (13) to perform a Kalman filter measurement update utilizing pseudo observations of velocity and roll:

$$\begin{aligned}\mathbf{S}_{k+1} &= \mathbf{H}_{k+1}^{\mathrm{ps}}\mathbf{P}_{k+1|k}(\mathbf{H}_{k+1}^{\mathrm{ps}})^\intercal + \mathbf{R}_{k+1}^{\mathrm{ps}},\\ \mathbf{K}_{k+1} &= \mathbf{P}_{k+1|k}(\mathbf{H}_{k+1}^{\mathrm{ps}})^\intercal \mathbf{S}_{k+1}^{-1},\\ \hat{\mathbf{x}}_{k+1|k+1} &= \hat{\mathbf{x}}_{k+1|k} - \mathbf{K}_{k+1}\mathbf{h}^{\mathrm{ps}}(\hat{\mathbf{z}}_{k+1|k}),\\ \mathbf{P}_{k+1|k+1} &= (\mathbf{I}_{18} - \mathbf{K}_{k+1}\mathbf{H}_{k+1}^{\mathrm{ps}})\mathbf{P}_{k+1|k}.\end{aligned}$$

4: Correct the navigation solution using the estimated errors. The rotation matrix update is given by (18) in the Appendix. The Euler angle estimates $\widehat{\boldsymbol{\psi}}_{\kappa_1\kappa_2}^{\kappa_1}$ are uniquely defined by the rotation matrix $\widehat{\mathbf{C}}_{\kappa_2}^{\kappa_1}$.

$$\begin{aligned}[\hat{\mathbf{z}}_{k+1|k+1}]_{1:6} &= [\hat{\mathbf{z}}_{k+1|k}]_{1:6} - [\delta\mathbf{z}_{k+1|k+1}]_{1:6},\\ \widehat{\mathbf{C}}_{s,k+1|k+1}^{t} &= (\delta\mathbf{C}_{s,k+1|k+1}^{t})^\intercal \widehat{\mathbf{C}}_{s,k+1|k}^{t},\\ \widehat{\mathbf{C}}_{b,k+1|k+1}^{s} &= (\delta\mathbf{C}_{b,k+1|k+1}^{s})^\intercal \widehat{\mathbf{C}}_{b,k+1|k}^{s}.\end{aligned}$$

where we use the notation

$$\delta\mathbf{y} \triangleq \begin{bmatrix}\mathbf{y}\\ \mathbf{0}_{3,1}\end{bmatrix} - \begin{bmatrix}\mathbf{h}^{\text{GNSS}}(\hat{\mathbf{z}})\\ \mathbf{h}^{\mathrm{ps}}(\hat{\mathbf{z}})\end{bmatrix}, \tag{15}$$

$\mathbf{H} \triangleq \big[(\mathbf{H}^{\text{GNSS}})^\intercal\ \ (\mathbf{H}^{\mathrm{ps}})^\intercal\big]^\intercal$, and $\mathbf{e}_k \triangleq [(\boldsymbol{\epsilon}_k)^\intercal\ (\boldsymbol{\epsilon}_k^{\mathrm{ps,v}})^\intercal\ \boldsymbol{\epsilon}_k^{\mathrm{ps},\phi}]^\intercal$, with $\mathbf{H}^{\text{GNSS}}$ and $\mathbf{H}^{\mathrm{ps}}$ defined in the Appendix. The measurement noise covariance matrix is

$$\begin{aligned}\mathbf{R} &\triangleq \operatorname{Cov}(\mathbf{e}_k)\\ &= \operatorname{blkdiag}(\mathbf{R}^{\text{GNSS}}, \mathbf{R}^{\mathrm{ps}}).\end{aligned} \tag{16}$$

Algorithm 1 displays one iteration of the filtering algorithm resulting from implementing an EKF based on (12) and (14), with $\mathbf{P}_{k_1|k_2}$ denoting the state covariance of $\hat{\mathbf{x}}_{k_1|k_2}$. The computational cost of the algorithm, not considering e.g., symmetry properties, will be dominated by a term in the order of $6d^3$ per iteration, where d denotes the dimension of the state vector [19]. Running the algorithm at $20\,[Hz]$ would then require $20 \cdot 6 \cdot 18^3\,[flops] \approx 0.7\,[Mflops]$, which is several orders of magnitude smaller than the maximum number of flops performed by standard smartphones.

It can be noted that the pseudo observations of roll (13b) are needed to fade out the effect the initial smartphone-to-vehicle roll angle (the value of ϕ_{sb}^s does not have any effect on the error estimates $\hat{\mathbf{x}}$ if only GNSS measurements and NHCs are employed). The design parameters $\sigma_{\mathrm{ps,v}}^2$ and $\sigma_{\mathrm{ps},\phi}^2$ describe the trade-off between allowing for vehicle dynamics which deviates from those implied by perfect measurements in (13), and increasing the ability to utilize the added information provided by the same equations.

The estimates of the smartphone's position and velocity will also be the estimates of the vehicle's position and velocity. This follows from making the assumption of zero relative position and velocity when utilizing the NHCs in the derivation of (14). While studies have been presented on how to estimate the smartphone-to-vehicle position [20], these assume that reference data is available either from the vehicle's on-board-diagnostics system, or from additional smartphone devices.

B. Initialization

The smartphone's position and velocity are initialized using the first available GNSS measurements, with the initial velocity in the vertical direction of the tangent frame set to zero. All sensor biases are initialized as zero.

It is convenient to express the initial attitudes as $\boldsymbol{\psi}_{ts,0}^t$ and $\boldsymbol{\psi}_{tb,0}^t$ and then compute $\boldsymbol{\psi}_{sb,0}^s$ from $\mathbf{C}_{b,0}^s = \mathbf{C}_{t,0}^s\mathbf{C}_{b,0}^t$, where $\mathbf{C}_{\kappa_1}^{\kappa_2}$ denotes the rotation matrix from frame κ_1 to frame κ_2. The first two elements in $\boldsymbol{\psi}_{ts,0}^t$ can be estimated from accelerometer measurements during presumed zero acceleration [15]. Moreover, the first two elements in $\boldsymbol{\psi}_{tb,0}^t$ are generally close to zero, and the yaw angle of the vehicle can be initialized from the first GNSS measurement of planar course.

The initial yaw angle of the smartphone typically has to be estimated by nonlinear methods. We choose to marginalize the navigation system in a marginalized particle filter (MPF), where each particle is associated with a unique initial state (refer to [21] for details on MPFs). Similar methods for other applications have previously been discussed in [22] and [23]. When sufficient weight has been distributed to one of the particles, the particle filter is terminated and the navigation system can continue with the identified initial state.

V. Simulation Study

We will now present the results of the conducted simulation study. True navigational data emulating typical vehicle dynamics was generated along the trajectory shown in Fig. 2. The corresponding horizontal speed is shown in Fig. 3. When generating the trajectory, the NHCs were utilized as hard equality constraints, so that the true vehicle dynamics satisifed $\mathbf{h}^{\mathrm{ps,v}}(\mathbf{z}_k) = \mathbf{0}_{2,1}$. Furter, the vehicle's roll angle was simulated as a zero mean, auto-regressive process of first order. Each run of the simulation generated a stationary smartphone-to-vehicle orientation, a constant IMU bias, and white, normally distributed sensor and measurement noise over the full trajectory. The update rates of the IMU sensor and the GNSS receiver were set to $20\,[Hz]$ and $1\,[Hz]$, respectively.

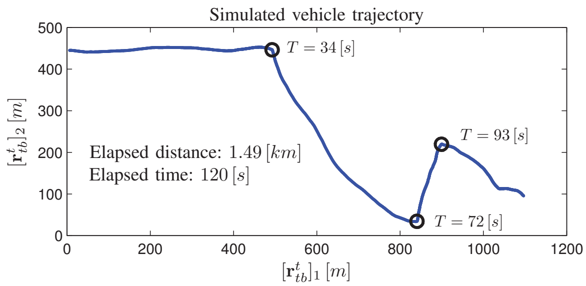

Fig. 2. Vehicle trajectory generated from Monte Carlo simulations.

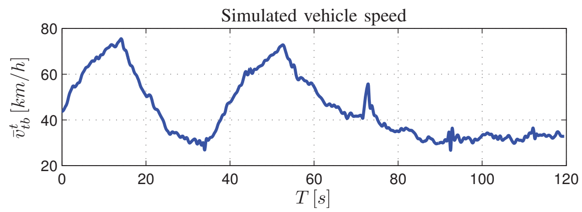

Fig. 3. Vehicle speed generated from Monte Carlo simulations.

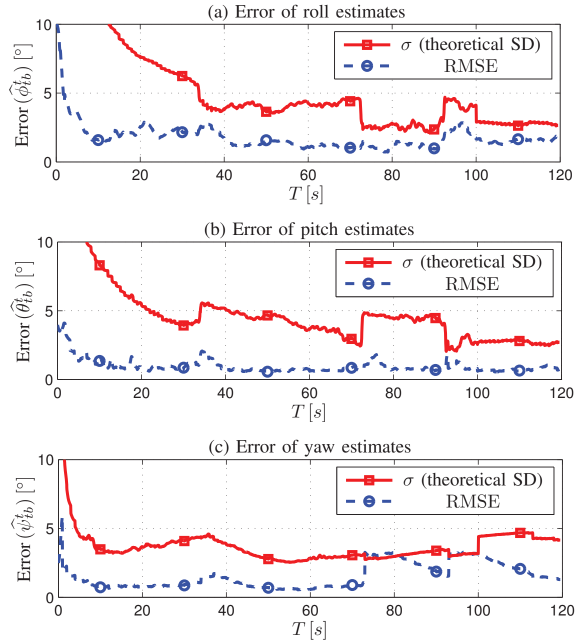

Fig. 4. Estimation errors of the vehicle's Euler angles.

The root-mean-square error (RMSE) and the theoretical standard deviation (SD) of each of the vehicle's Euler angles are shown in Fig. 4. The displayed figures are the result of 100 Monte Carlo realizations. The SDs were obtained by employing the approximation (readily obtained from (26) in the Appendix)

$$\begin{aligned}\text{Cov}(\delta\boldsymbol{\psi}^t_{tb}) \approx \text{Cov}(\delta\boldsymbol{\psi}^t_{ts}) &+ \widehat{\mathbf{C}}^t_s\text{Cov}(\delta\boldsymbol{\psi}^s_{sb}, \delta\boldsymbol{\psi}^t_{ts}) \\ &+ (\widehat{\mathbf{C}}^t_s\text{Cov}(\delta\boldsymbol{\psi}^s_{sb}, \delta\boldsymbol{\psi}^t_{ts}))^\intercal + \widehat{\mathbf{C}}^t_s\text{Cov}(\delta\boldsymbol{\psi}^s_{sb})\widehat{\mathbf{C}}^s_t\end{aligned} \tag{17}$$

in each simulation, and then computing the average of the corresponding standard deviations at each sampling instance. Here, $\text{Cov}(\cdot)$ and $\text{Cov}(\cdot,\cdot)$ denote the covariance matrix of a random vector and the cross-covariance matrix of two random vectors, respectively. Note that all covariance and cross-covariance matrices in the right-hand-side of (17) can be obtained as sub-matrices of the state covariance matrix $\mathbf{P}$.

As indicated in Fig. 4, convergence typically occurs within 60 seconds, with a steady state RMSE in the order of $2\,[°]$ for each Euler angle. For comparison, it can be noted that estimating the roll and pitch angles as $0\,[°]$ at each sampling instance would result in a time-averaged RMSE of $5.74\,[°]$ and $4.29\,[°]$, respectively. The simulations employed the same filter as was used for the experimental data in Section VI, and hence, the theoretical SDs generally exceed the RMSEs. This is a consequence of filtering with a nonzero measurement noise covariance in the pseudo observations of velocity, and nonzero process noise covariance in the time development of $\boldsymbol{\psi}^s_{sb,k}$.

The exact error graphs in Fig. 4 will be highly dependent on the vehicle dynamics. As an example, the estimates of the roll and pitch angles can be seen to exchange information uncertainty as the vehicle changes course (consider e.g., the change in theoretical SD of the roll and pitch estimates when the vehicle corners at $T = 72\,[s]$). This can be attributed to the fact that the system's observability varies with the vehicle dynamics. Refer to e.g., [24] for details on the observability of GNSS-aided INSs during different vehicle maneuvers.

VI. Field Study

The algorithm presented in Section IV was applied to 25 minutes of driving data collected from a Samsung S3, a Samsung S4, and an iPhone 5, all fixed to the dashboard but with an unknown orientation. Simultaneously, reference data was collected using a Microstrain 3DM-GX3-35 aligned to the vehicle's coordinate frame. The update rates of the IMUs were set to $20\,[Hz]$, while the GNSS receivers of the smartphones and the reference system were operating at update rates of $1\,[Hz]$ and $4\,[Hz]$, respectively. The reference data was processed in a standard GNSS-aided INS. Due to limitations in the accuracy of the reference system, the presented results should be considered as an indication of achievable performance, rather than as exact measures. Although the presented framework does not explicitly require the smartphone to be fixed with respect to the vehicle, convergence is, according to the authors' experience, difficult to achieve when the smartphone is rotating with respect to vehicle. However, since the angular velocity measured when a user picks up the smartphone generally is much larger than any angular velocity caused by vehicle maneuvers, sporadic user initiated movements should be possible to filter out as described in Section I.

The time-averaged RMSEs of the vehicle's Euler angle estimates are shown in Table I, and can be seen to be in the same order as the RMSEs obtained in the simulation study in Section V. Further, Fig. 5 displays the position drifts during simulated GNSS outages, in terms of the root-mean-square horizontal position error $\text{RMSE}([\hat{\mathbf{r}}^t_{tb}]_{1:2})$. Outages were simulated by

TABLE I
ROOT-MEAN-SQUARE-ERRORS OF VEHICLE ANGLES.

	Samsung S3	Samsung S4	iPhone 5
ϕ_{tb}^{t} [°]	0.86	0.96	1.49
θ_{tb}^{t} [°]	0.87	0.86	1.29
ψ_{tb}^{t} [°]	2.36	2.08	3.21

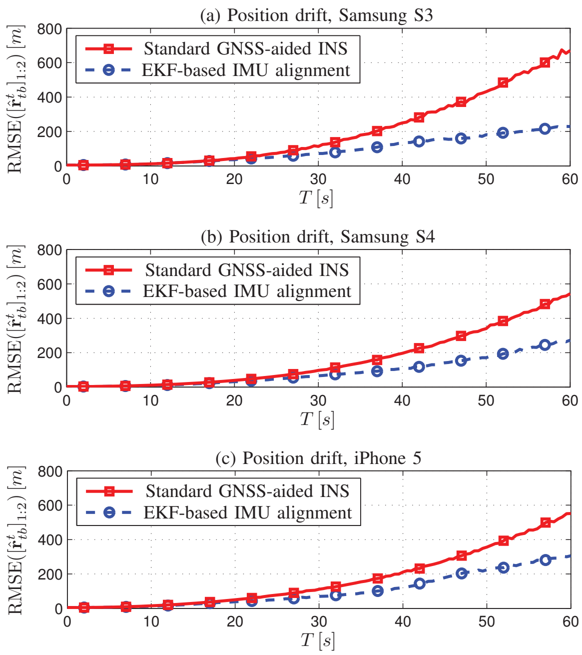

Fig. 5. Position drifts during GNSS outage as dependent on the time length of the outage.

removing GNSS data from sequential periods of 60 seconds, starting 240 seconds after start-up and continuing up until the end of the data set. The proposed IMU alignment method was run several times with GNSS measurements removed from one of the periods in each run. For comparison, the corresponding position drifts resulting from applying the standard 15-state GNSS-aided INS to each smartphone are also shown. As seen from Fig. 5, the IMU alignment method reduces the position error growth considerably for each of the three smartphones. This confirms that the pseudo observations of velocity and roll provide the navigation system with valuable information despite small errors in the estimated smartphone-to-vehicle orientation. Noteworthy is that the error drift is still quite large due to the poor quality of the inertial sensors in the smartphones.

VII. CONCLUSIONS

This paper has presented a method for simultaneous vehicle navigation and smartphone-to-vehicle alignment, which can be seen as an extension of the standard GNSS-aided INS. The alignment is performed by applying NHCs with the smartphone-to-vehicle orientation as an unknown state element. The accuracy of the estimated vehicle attitude is in the order of 2 [°] for each Euler angle, with convergence occuring within minutes. It was further shown that the proposed method reduce the position error growth during GNSS outages.

With reliable estimates of the relative smartphone-to-vehicle orientation, measurements from the smartphone's inertial measurement unit can be utilized in the same way as if the smartphone had been manually aligned to the vehicle frame. Hence, the proposed method opens up a wide range of applications utilizing smartphone-based inertial measurements for automotive navigation, without setting any requirements on the smartphone's orientation with respect to the vehicle.

APPENDIX

This appendix derives the linearized measurement matrix $\mathbf{H}_k$ and the measurement error $\delta\mathbf{y}_k$ in (14) by linearizing the measurements (10b) and (13) around $\hat{\mathbf{z}}$. We will use that

$$\delta\mathbf{C}_{\kappa_2}^{\kappa_1} \triangleq \widehat{\mathbf{C}}_{\kappa_2}^{\kappa_1}\mathbf{C}_{\kappa_1}^{\kappa_2} \tag{18}$$

where $\widehat{\mathbf{C}}_{\kappa_2}^{\kappa_1}$ and $\mathbf{C}_{\kappa_1}^{\kappa_2}$ are uniquely defined by $\widehat{\boldsymbol{\psi}}_{\kappa_1\kappa_2}^{\kappa_1}$ and $\boldsymbol{\psi}_{\kappa_1\kappa_2}^{\kappa_1}$, respectively, while $\delta\mathbf{C}_{\kappa_2}^{\kappa_1}$ defines $\delta\boldsymbol{\psi}_{\kappa_1\kappa_2}^{\kappa_1}$ through the small angle approximation

$$[\delta\boldsymbol{\psi}_{\kappa_1\kappa_2}^{\kappa_1}]^{\times} \triangleq \delta\mathbf{C}_{\kappa_2}^{\kappa_1} - \mathbf{I}_3. \tag{19}$$

Here, $[\mathbf{c}]^{\times}$ is the skew symmetric matrix defined such that $[\mathbf{c}_1]^{\times}\mathbf{c}_2$ is equal to the cross product of $\mathbf{c}_1$ and $\mathbf{c}_2$.

First, we approximate the measurement function in (10b) as

$$\begin{aligned}\mathbf{h}^{\text{GNSS}}(\bar{\mathbf{z}}) &\approx \mathbf{h}^{\text{GNSS}}(\hat{\bar{\mathbf{z}}}) + \frac{\partial\mathbf{h}^{\text{GNSS}}(\hat{\bar{\mathbf{z}}})}{\partial\bar{\mathbf{z}}}(\bar{\mathbf{z}} - \hat{\bar{\mathbf{z}}})\\ &= \mathbf{h}^{\text{GNSS}}(\hat{\bar{\mathbf{z}}}) + \frac{\partial\mathbf{h}^{\text{GNSS}}(\hat{\bar{\mathbf{z}}})}{\partial\mathbf{x}}\mathbf{x}\end{aligned} \tag{20}$$

which gives

$$\mathbf{y} - \mathbf{h}^{\text{GNSS}}(\hat{\bar{\mathbf{z}}}) \approx \mathbf{H}^{\text{GNSS}}\mathbf{x} + \boldsymbol{\epsilon} \tag{21}$$

where

$$\begin{aligned}\mathbf{H}^{\text{GNSS}} &\triangleq \frac{\partial\mathbf{h}^{\text{GNSS}}(\hat{\bar{\mathbf{z}}})}{\partial\mathbf{x}}\\ &= \begin{bmatrix} -\dfrac{\partial\mathbf{h}^{\text{GNSS}}(\hat{\bar{\mathbf{z}}})}{\partial\bar{\mathbf{z}}} & \mathbf{0}_{5,9}\end{bmatrix}\\ &= -\begin{bmatrix}\mathbf{I}_3 & \mathbf{0}_{3,1} & \mathbf{0}_{3,1} & \mathbf{0}_{3,13}\\ \mathbf{0}_{1,3} & [\hat{\mathbf{v}}_{ts}^{t}]_1/\bar{\mathrm{v}}_{ts}^{t} & [\hat{\mathbf{v}}_{ts}^{t}]_2/\bar{\mathrm{v}}_{ts}^{t} & \mathbf{0}_{1,13}\\ \mathbf{0}_{1,3} & -[\hat{\mathbf{v}}_{ts}^{t}]_2/(\hat{\bar{\mathrm{v}}}_{ts}^{t})^2 & [\hat{\mathbf{v}}_{ts}^{t}]_1/(\hat{\bar{\mathrm{v}}}_{ts}^{t})^2 & \mathbf{0}_{1,13}\end{bmatrix}.\end{aligned} \tag{22}$$

Moving on to the pseudo observations of velocity in (13a) and assuming $\mathbf{r}_{bs}^{(\cdot)} \approx 0$ and $\mathbf{v}_{bs}^{(\cdot)} \approx 0$, we have

$$\begin{aligned}\mathbf{v}_{tb}^{b} &= \mathbf{C}_s^b\mathbf{C}_t^s\mathbf{v}_{tb}^{t}\\ &\approx \mathbf{C}_s^b\mathbf{C}_t^s\mathbf{v}_{ts}^{t}\\ &= \widehat{\mathbf{C}}_s^b\delta\mathbf{C}_b^s\widehat{\mathbf{C}}_t^s\delta\mathbf{C}_s^t(\hat{\mathbf{v}}_{ts}^{t} - \delta\mathbf{v}_{ts}^{t})\\ &= \widehat{\mathbf{C}}_s^b(\mathbf{I}_3 + [\delta\boldsymbol{\psi}_{sb}^{s}]^{\times})\widehat{\mathbf{C}}_t^s(\mathbf{I}_3 + [\delta\boldsymbol{\psi}_{ts}^{t}]^{\times})(\hat{\mathbf{v}}_{ts}^{t} - \delta\mathbf{v}_{ts}^{t})\\ &\approx \widehat{\mathbf{C}}_s^b\widehat{\mathbf{C}}_t^s(\hat{\mathbf{v}}_{tb}^{t} - \delta\mathbf{v}_{ts}^{t} + [\delta\boldsymbol{\psi}_{ts}^{t}]^{\times}\hat{\mathbf{v}}_{ts}^{t}) + \widehat{\mathbf{C}}_s^b[\delta\boldsymbol{\psi}_{sb}^{s}]^{\times}\widehat{\mathbf{C}}_t^s\hat{\mathbf{v}}_{ts}^{t}\\ &= \hat{\mathbf{v}}_{tb}^{b} - \widehat{\mathbf{C}}_s^b\widehat{\mathbf{C}}_t^s(\delta\mathbf{v}_{ts}^{t} + [\hat{\mathbf{v}}_{ts}^{t}]^{\times}\delta\boldsymbol{\psi}_{ts}^{t}) - \widehat{\mathbf{C}}_s^b[\widehat{\mathbf{C}}_t^s\hat{\mathbf{v}}_{ts}^{t}]^{\times}\delta\boldsymbol{\psi}_{sb}^{s}\end{aligned} \tag{23}$$

and hence, we can write

$$\mathbf{0}_{2,1} - \mathbf{h}^{\text{ps,v}}(\hat{\mathbf{z}}) \approx \mathbf{H}^{\text{ps,v}}\mathbf{x} + \boldsymbol{\epsilon}^{\text{ps,v}} \tag{24}$$

where

$$\mathbf{H}^{\mathrm{ps,v}} \triangleq -\mathbf{A}\big[\mathbf{0}_{3,3} \;\; \widehat{\mathbf{C}}_s^b\widehat{\mathbf{C}}_t^s \;\; \widehat{\mathbf{C}}_s^b\widehat{\mathbf{C}}_t^s[\hat{\mathbf{v}}_{ts}^t]^\times \;\; \widehat{\mathbf{C}}_s^b[\widehat{\mathbf{C}}_t^s\hat{\mathbf{v}}_{ts}^t]^\times \;\; \mathbf{0}_{3,6}\big]. \tag{25}$$

For the pseudo observations of roll in (13b) we note that

$$\begin{aligned}[\delta\boldsymbol{\psi}_{tb}^t]^\times &= \widehat{\mathbf{C}}_b^t\mathbf{C}_t^b - \mathbf{I}_3\\ &= \widehat{\mathbf{C}}_s^t\widehat{\mathbf{C}}_b^s\mathbf{C}_s^b\mathbf{C}_t^s - \mathbf{I}_3\\ &= \widehat{\mathbf{C}}_s^t\mathbf{C}_t^s + \widehat{\mathbf{C}}_s^t[\delta\boldsymbol{\psi}_{sb}^s]^\times\mathbf{C}_t^s - \mathbf{I}_3\\ &\approx [\delta\boldsymbol{\psi}_{ts}^t]^\times + \widehat{\mathbf{C}}_s^t[\delta\boldsymbol{\psi}_{sb}^s]^\times\widehat{\mathbf{C}}_t^s\end{aligned} \tag{26}$$

which further gives

$$\begin{aligned}\boldsymbol{\psi}_{tb}^t &\approx \widehat{\boldsymbol{\psi}}_{tb}^t - \delta\boldsymbol{\psi}_{tb}^t\\ &\approx \widehat{\boldsymbol{\psi}}_{tb}^t - \delta\boldsymbol{\psi}_{ts}^t - \widehat{\mathbf{C}}_s^t\delta\boldsymbol{\psi}_{sb}^s.\end{aligned} \tag{27}$$

This results in

$$0 - \mathbf{h}^{\mathrm{ps},\phi}(\hat{\mathbf{z}}) \approx \mathbf{H}^{\mathrm{ps},\phi}\mathbf{x} + \boldsymbol{\epsilon}^{\mathrm{ps},\phi} \tag{28}$$

where

$$\mathbf{H}^{\mathrm{ps},\phi} \triangleq -\mathbf{b}^\intercal\big[\mathbf{0}_{3,6} \quad \mathbf{I}_3 \quad \widehat{\mathbf{C}}_s^t \quad \mathbf{0}_{3,6}\big]. \tag{29}$$

The linearized measurement matrix $\mathbf{H}$ in (14) can now be obtained from

$$\mathbf{H}^{\mathrm{ps}} \triangleq \big[(\mathbf{H}^{\mathrm{ps,v}})^\intercal \;\; (\mathbf{H}^{\mathrm{ps},\phi})^\intercal\big]^\intercal. \tag{30}$$

REFERENCES

[1] I. Skog and P. Händel, “In-car positioning and navigation technologies - A survey,” *IEEE Trans. Intell. Transport. Syst.*, vol. 10, no. 1, pp. 4–21, Mar. 2009.

[2] J. C. Herrera, “Assessment of GPS-enabled smartphone data and its use in traffic state estimation for highways,” University of California, Berkeley, Tech. Rep., 2009.

[3] R. Zantout, M. Jrab, L. Hamandi, and F. Sibai, “Fleet management automation using the global positioning system,” in *Int. Conf. Innovations Inf. Technol.*, Al Ain, United Arab Emirates, Dec. 2009, pp. 30–34.

[4] A. Corti, V. Manzoni, S. Savaresi, M. Santucci, and O. Di Tanna, “A centralized real-time driver assistance system for road safety based on smartphone,” in *Advanced Microsystems for Automotive Applications*. Springer Berlin Heidelberg, 2012, pp. 221–230.

[5] P. Händel, I. Skog, J. Wahlström, F. Bonawiede, R. Welch, J. Ohlsson, and M. Ohlsson, “Insurance telematics: Opportunities and challenges with the smartphone solution,” *IEEE Intell. Transport. Syst. Mag.*, vol. 6, no. 4, pp. 57–70, Oct. 2014.

[6] J. Paefgen, F. Kehr, Y. Zhai, and F. Michahelles, “Driving behavior analysis with smartphones: insights from a controlled field study,” in *Proc. 11th Mobile and Ubiquitous Multimedia Conf.*, Luleå, Sweden, Dec. 2012, pp. 36:1–8.

[7] J. Almazan, L. Bergasa, J. Yebes, R. Barea, and R. Arroyo, “Full auto-calibration of a smartphone on board a vehicle using IMU and GPS embedded sensors,” in *Proc. IEEE 4th Symp. Intell. Veh.*, Gold Coast City, Australia, Jun. 2013, pp. 1374–1380.

[8] X. Niu, Q. Zhang, Y. Li, Y. Cheng, and C. Shi, “Using inertial sensors of iPhone 4 for car navigation,” in *Proc. IEEE/ION Position, Location Navig. Symp.*, Myrtle Beach, SC, Apr. 2012, pp. 555–561.

[9] P. Mohan, V. N. Padmanabhan, and R. Ramjee, “Trafficsense: Rich monitoring of road and traffic conditions using mobile smartphones,” Microsoft Research, Tech. Rep., Apr. 2008.

[10] N. Promwongsa, P. Chaisatsilp, S. Supakwong, C. Saiprasert, T. Pholprasit, and P. Prathombutr, “Automatic accelerometer reorientation for driving event detection using smartphone,” in *Proc. 13th ITS Asia Pacific Forum*, Auckland, New Zealand, Apr. 2014.

[11] D. Johnson and M. Trivedi, “Driving style recognition using a smartphone as a sensor platform,” in *IEEE Conf. Intell. Transport. Syst.*, Washington, DC, Oct. 2011, pp. 1609–1615.

[12] K. Yagi, “Extensional smartphone probe for road bump detection,” in *Proc. 17th Intell. Transport. Syst. World Congress*, Busan, Korea, Oct. 2010.

[13] M. Reineh, M. Enqvist, and F. Gustafsson, “Detection of roof load for automotive safety systems,” in *Proc. Conf. Decis. Contr.*, Florence, Italy, Dec. 2013, pp. 2840–2845.

[14] S. Sukkarieh, “Low cost, high integrity, aided inertial navigation systems for autonomous land vehicles,” Department of Mechanical and Mechatronic Engineering, The University of Sydney, Tech. Rep., Mar. 2000.

[15] J. Farrell, *Aided Navigation: GPS with High Rate Sensors*, 1st ed. New York, NY: McGraw-Hill, Inc., 2008.

[16] P. D. Groves, *Principles of GNSS, inertial, and multisensor integrated navigation systems*, 1st ed. Artech House, 2008.

[17] J. Wahlström, I. Skog, and P. Händel, “Detection of dangerous cornering in GNSS data driven insurance telematics,” *Accepted in IEEE Trans. Intell. Transport. Syst.*

[18] D. Simon, “Kalman filtering with state constraints: a survey of linear and nonlinear algorithms,” *IET Control Theory Appl.*, vol. 4, no. 8, pp. 1303–1318, Aug. 2010.

[19] J. Mendel, “Computational requirements for a discrete Kalman filter,” *IEEE Trans. Autom. Control*, vol. 16, no. 6, pp. 748–758, Dec. 1971.

[20] Y. Wang, J. Yang, H. Liu, Y. Chen, M. Gruteser, and R. P. Martin, “Sensing vehicle dynamics for determining driver phone use,” in *Proc. 11th Annu. Int. Conf. Mobile Systems, Appl., Services*, New York, NY, Jun. 2013, pp. 41–54.

[21] T. B. Schön, “Estimation of nonlinear dynamic systems - theory and applications,” Ph.D. dissertation, Linköping University, 2006.

[22] J.-O. Nilsson and P. Händel, “Recursive bayesian initialization of localization based on ranging and dead reckoning,” in *Proc. IEEE, Intell. Robots and Syst. Int. Conf.*, Tokyo, Japan, Nov. 2013, pp. 1399–1404.

[23] T. B. Schön, A. Wills., and B. Ninness., “Maximum likelihood nonlinear system estimation,” in *Proc. 14th IFAC Symp.on Syst. Identification*, Newcastle, Australia, Mar. 2006, pp. 1003–1008.

[24] I. Rhee, M. Abdel-Hafez, and J. Speyer, “Observability of an integrated GPS/INS during maneuvers,” *IEEE Trans. Aerosp. Electron. Syst.*, vol. 40, no. 2, pp. 526–535, Apr. 2004.